

Summer Deep Depressions Increase Over the Eastern North Atlantic

Fabio D'Andrea¹, Fabio D'andrea^{2,3}, Jean-Philippe Duvel^{2,3}, Gwendal Rivière^{2,3}, Robert Vautard⁴, Christophe Cassou^{2,3,5}, Julien Cattiaux^{6,7,8}, Davide Faranda^{2,3,4,9}, Tamara Hapè⁶, Aglaé Jézéquel^{2,3}, Aurelien Ribes⁷, and Pascal Yiou⁹

¹Affiliation not available

²Laboratoire de Météorologie Dynamique/IPSL, ENS, PSL Research University

³Institut Polytechnique de Paris, Sorbonne Université, CNRS

⁴Institut Pierre-Simon Laplace, CNRS, Université Paris-Saclay, Sorbonne Université

⁵Centre Européen de Recherche et de Formation Avancée en Calcul Scientifique, UMR 5318, CNRS

⁶Institute for Environmental Studies, Vrije Universiteit Amsterdam

⁷CNRM

⁸Royal Netherlands Meteorological Institute (KNMI)

⁹Laboratoire des Sciences du Climat et de l'Environnement, UMR 8212 CEA-CNRS-UVSQ, Université Paris-Saclay and IPSL

March 07, 2024

1
2
3
4
5
6
7
8
9
10
11
12
13
14
15
16
17
18
19
20
21
22
23
24
25

Summer Deep Depressions Increase Over the Eastern North Atlantic

Fabio D’Andrea¹, Jean-Philippe Duvel¹, Gwendal Rivière¹, Robert Vautard², Christophe Cassou^{1,4}, Julien Cattiaux⁵, Dim Coumou^{3,7,2}, Davide Faranda^{1,6}, Tamara Happé³, Aglaé Jézéquel¹, Aurelien Ribes⁵, Pascal Yiou⁶.

¹ Laboratoire de Météorologie Dynamique/IPSL, ENS, PSL Research University, École Polytechnique, Institut Polytechnique de Paris, Sorbonne Université, CNRS, Paris France

² Institut Pierre-Simon Laplace, CNRS, Université Paris-Saclay, Sorbonne Université, France

³ Institute for Environmental Studies, Vrije Universiteit Amsterdam, Amsterdam, Netherlands

⁴ Centre Européen de Recherche et de Formation Avancée en Calcul Scientifique, CNRS UMR 5318, Toulouse, France

⁵ CNRM, Toulouse

⁶ Laboratoire des Sciences du Climat et de l’Environnement, UMR 8212 CEA-CNRS-UVSQ, Université Paris-Saclay and IPSL, 91191 Gif-sur-Yvette, France

⁷ Royal Netherlands Meteorological Institute (KNMI), De Bilt, Netherlands

Corresponding author: Fabio D’Andrea (dandrea@lmd.ipsl.fr)

Key Points:

- Deep depression occurrences have significantly increased over the eastern side, and decreased over the western side of the North Atlantic.
- Deep depressions are linked to high surface temperature patterns in western continental Europe but have little impact on the mean warming.
- Global Climate Models fail to reproduce the observed trends in deep depressions correctly

26 **Abstract**

27 Mid-tropospheric deep depressions in summer over the North Atlantic are shown to have strongly
28 increased in the eastern and strongly decreased in the western North Atlantic region. This evolution is
29 linked to a change in baroclinicity in the west of the North Atlantic ocean and over the North American
30 coast, likely due to the increased surface temperature there. Deep depressions in the Eastern North
31 Atlantic are linked to a temperature pattern typical of extreme heat events in the region. The same
32 analysis is applied to a sample of CMIP6 model outputs, and no such trends are found. This study
33 suggests a link between the observed increase of summer extreme heat events in the region and the
34 increase of the number of Atlantic depressions. The failure of CMIP6 models to reproduce these events
35 can consequently also reside in an incorrect reproduction of this specific feature of midlatitude
36 atmospheric dynamics.

37 **Plain Language Summary**

38 Extreme temperatures events in Western Europe have been rising fast, and current global climate models
39 are not able to reproduce this excess. There are different hypotheses to explain this discrepancy. One is
40 that the large-scale atmospheric dynamics, responsible for the local weather, is not correctly represented
41 by the models: indeed, the frequency and amplitude of some specific weather phenomena have been
42 shown to be insufficiently reproduced, especially in summer. Here, we study one such phenomenon,
43 namely the transient deep depressions, or extratropical cyclones, that travel across the Atlantic basin. A
44 significant large increase of the number of these events is found in summer in the region of the North
45 Atlantic off the western European coast. Depressions in that region are accompanied by high temperatures
46 in continental western Europe. An ensemble of state of the art climate models are also analyzed and none
47 of them is able to correctly reproduce the frequency of deep depressions nor their large trend, which
48 suggests a common origin with the insufficient prediction of western European extreme heat events. Great
49 caution should be used when analyzing climate change predictions in the region, and even more so when
50 studying changes in complex dynamical phenomena.

51 **1 Introduction**

52 Climate has been warming quickly in Western Europe. Over mainland France, for instance, mean daily
53 temperatures estimated over the 1950-2022 period, show an increase of more than 1.5°C as a response to
54 climate change (Ribes et al 2022), and mean daily maximum temperatures in the region have been
55 measured to increase twice to three times as much as the global mean (Vautard et al 2023). More notably,
56 heatwaves are increasing, as illustrated by several unprecedented events in the last 20 years, with a
57 number of observed record-breaking temperatures exceeding those expected in a stationary climate
58 (Bador et al, 2016). While climate projections show an increase of extreme temperatures in Western
59 Europe with climate change, the amplitude is only captured by very few current climate simulations (van
60 Oldenborgh et al 2009, Boé et al 2020, Ribes et al 2022, van Oldenborgh et al. 2022).
61 There is growing evidence that this amplified warming is a result of changes in atmospheric circulation.
62 Using circulation analogues, Vautard et al (2023) distinguished atmospheric patterns likely to explain
63 such discrepancy, where large scale zonal pressure gradient systems enhance southerly flow and
64 anticyclonic conditions over the continent. A similar pattern encompassing a low-pressure system (named
65 a *depression* hereafter) over the eastern Atlantic was found by Faranda et al (2023), still by an analogue
66 approach on historical data, as the pattern with the highest increase in frequency in the region, always
67 linked to extreme temperatures. Southerly advection is not the only mechanism that potentially explains
68 how Atlantic depressions can bring about a warming of continental Europe. On a heatwave case study,
69 Zschenderlein et al (2019) showed that upper tropospheric ridges on the eastern flank of a depression can
70 prevail over horizontal advection of temperature, via enhanced adiabatic heating by subsidence, or also by
71 diabatic heating at the surface. Indeed, in recent times a number of persistent depressions off the
72 European Atlantic coast have accompanied high or even record breaking temperatures at different
73 locations over the continent. The events of June 2019 and July 2022 made headlines in the mainstream

74 press. Diabatic heating in the storm track upstream of a blocking anticyclone can also bring additional
75 upper-level heat into the block, such as in the Pacific-Northwest American heatwave of 2021
76 (Schumacher et al., 2022).

77 Motivated by the above works, we develop a simple objective algorithm to count and characterize deep
78 depressions, and we apply it to the Atlantic/European region in summer. The focus of this paper is to
79 investigate the synoptic aspects of the depressions and their long term evolution in up-to-date reanalysed
80 and modeled data. Analysing their precise physical link with heatwaves is deferred to a forthcoming
81 paper. In previous literature, extratropical depressions are comparatively less studied in summer, and
82 never in the context of high temperature events in Europe; a review can be found in Freser et al (2015). In
83 section 2, the algorithm is described in detail, as well as the data used. In section 3, the algorithm is
84 applied to reanalysed geopotential fields for the whole North Atlantic region and the results are compared
85 to the storm track and baroclinicity. In section 4, attention is concentrated on the region of the Eastern
86 Atlantic where the strongest evolution of the number of depressions is found; temperature composites are
87 also shown. In section 5 an ensemble of global climate models outputs is analyzed with the same
88 methodology. Section 6 is where the results are summarized and discussed with some detail.

89 **2 Data and Methods**

90 Reanalysed data from ERA5 (Hersbach et al. 2020) are used for the Northern summer months of June July
91 and August (JJA) from 1950 to 2022. Hourly Geopotential fields at 500 hPa (z500) are used with a time
92 step of 24h hours, at 12 UTC at a grid resolution of 0.25 degrees. Depressions are identified from minima
93 of z500 anomalies; the precise methodology is detailed below. The NCEP reanalysis (Kalnay et al., 1996)
94 is also used in the same manner for comparison, but the main analysis is shown for ERA5.

95 The region considered covers the North Atlantic and Europe. Long term trends in the number of days with
96 depression occurrence and the long-term dynamical change are analyzed. Successively, a region in the
97 Eastern Atlantic off the Western European coast is singled out, and the composites of temperature maps are
98 computed.

99 The depression search has also been applied to the output of climate models participating in the Coupled
100 Model Intercomparison Project 6 (CMIP6, Eyring et al, 2020). The list of the models analyzed, with some
101 additional information is found in the supplementary material (Table S1). The daily z500 output of all
102 models was re-interpolated on the same grid as ERA5, and then the algorithm as described below has been
103 applied.

104 The precise methodology used is detailed as follows:

105 1) We consider squares of $15^\circ \times 15^\circ$ in the Euro-Atlantic region with an increment of 1° of latitude and
106 longitude between 65° and 20° N and between 80° W and 20° E.

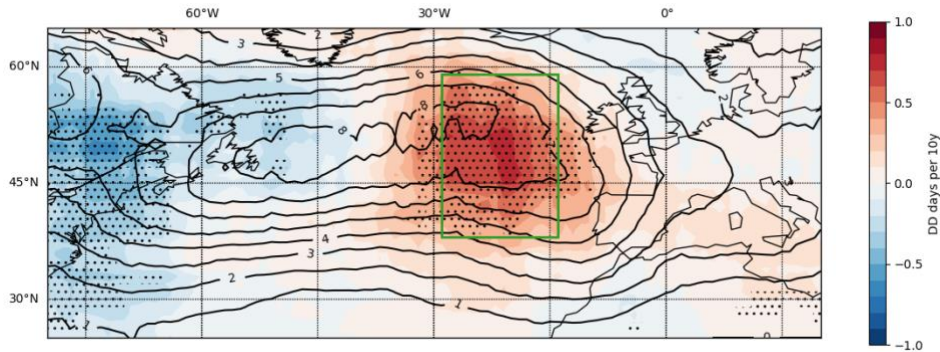
107 2) The minimum z500 anomaly with respect to long term mean is found in each square.

108 3) The minimum is tested for depth (refer to the schematics in Sec 1.1 of the supplementary material):
109 starting from the gridpoint of the minimum, we consider a segment of $\Delta\lambda=10$ degrees of longitude or
110 latitude in the four cardinal directions. Along the segment we select the maximum z500 anomaly; if the
111 difference between this maximum and the central minimum exceeds an amplitude $A=110$ meters in all the
112 directions, we retain it as a deep depression (DD).

113 4) If a given day has a DD selected, it is retained as a DD-day for the central point of the square of $15^\circ \times 15^\circ$
114 in longitude-latitude.

115 There are two arbitrary parameters in this algorithm: A and $\Delta\lambda$. The value of $A=110$ meters is chosen
116 according to the distribution of all depths of z500 minima in the region over the Eastern Atlantic described
117 in section 3 below; 110m corresponds to the 75th centile. The width $\Delta\lambda$ is not a very sensitive parameter.
118 More details on the choice of the parameters and sensitivity to their changes are found in the supplementary
119 material Sec. 10.

120

121 **3 Trend in Deep Depression Days**

122

123 *Figure 1. Average number of DD-days per summer (contours) and slope of the linear trend in the*
 124 *number of DD expressed as days per ten years (colors). Hatching indicates regions for which the trend is*
 125 *significant to a Mann-Kendall test with $p < 0.05$. The green rectangle indicates the chosen region for the*
 126 *analysis in Sec. 4.*

127

128 The result of the search for deep depressions in the Euro Atlantic region is shown in Fig. 1. The average
 129 number of DD-days per summer is maximum approximately along the mean location of the summer
 130 storm track region (Fig. 2A). A positive and statistically significant ($p < 0.05$) trend is found East-
 131 Southeast of the maximum. Conversely, a significantly negative linear trend is found west of the domain,
 132 along the north American eastern coast.

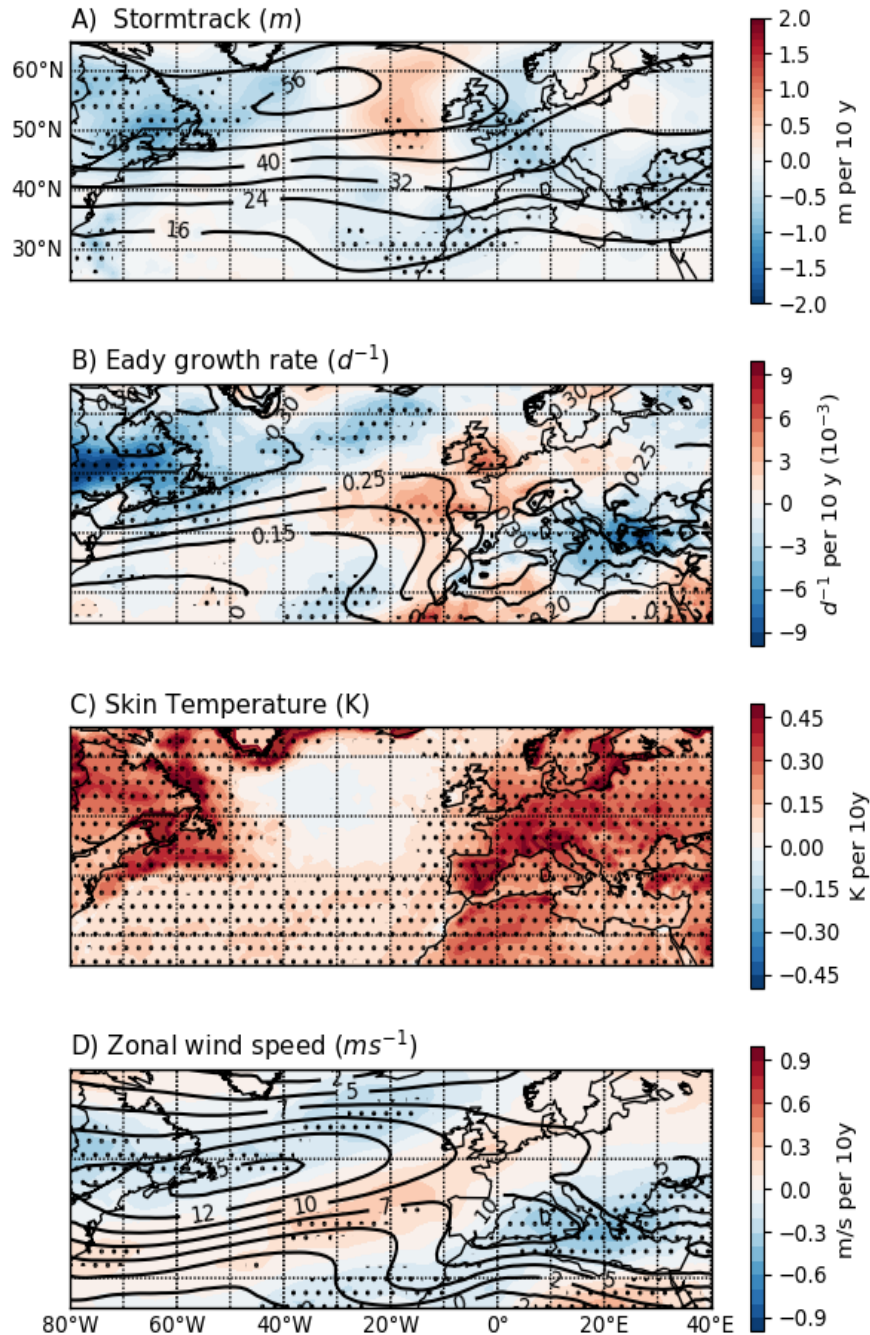
133 Climatological studies of extratropical cyclones make use of different metrics, based e.g. on relative or
 134 potential vorticity, and have methods for tracking trajectories on top of criteria for displacement speed
 135 and lifetime, so that a direct comparison with the present work is not straightforward. A comparison of
 136 different cyclone tracking methods is found in Raible et al (2008). They found for summer between 5 and
 137 15 cyclones per square of 1000 km of side and a pattern similar to the solid lines of Fig. 1. (see e.g. their
 138 figure 2). The trend shown in Fig. 1 is computed on the whole ERA5 period, which means that along the
 139 73 years there is practically a doubling of the number of summer DD-days at the location of the maximum
 140 trend and around. The field significance of Fig.1 has also been tested as in Wilks (2016), see
 141 supplementary material section 9. In the following, the trends of other physical variables are shown in the
 142 region.

143 The summer stormtrack activity, defined in a classical way as the 2-7 days band pass filtered standard
 144 deviation, is shown in Fig. 2A for z_{500} . It shows a significant - albeit smaller - linear trend entirely
 145 consistent with the evolution in the number of DD-days: negative on the west and positive in the
 146 east/southeast. This shift of the summer stormtrack was also observed by Deng et al (2022) along with the
 147 shift in position of the jet that will be discussed below. The decrease of stormtrack activity in the
 148 baroclinic region of the American East continental coast is explained by the reduced baroclinicity,
 149 measured by use of the Eady growth rate σ as defined in Hoskins and Valdes (1990):

150
$$\sigma = \alpha f \left| \frac{\partial u}{\partial z} \right| N^{-1}$$
, where N is the Brunt-Vaisala frequency. The Eady growth rate is computed for the
 151 850-500 hPa layer; f is the Coriolis parameter, u is the wind speed vector, and α is a factor, estimated to
 152 0.31 by Lindzen and Farrell (1980) from maximum growth rate in baroclinic instability problems.

153 The Eady growth rate is shown in Fig. 2B. It strongly decreases over Labrador and along the American
 154 continental coast. This is explained by the strong increase in surface temperature, visible on Fig. 2C, that
 155 creates a diminished meridional temperature gradient at higher levels, reducing the wind shear. This is
 156 better visible in the maps of temperature trends at higher levels, that are shown in the supplementary

157 material Fig. S6. Note that the change in σ is largely dominated everywhere by the change in wind shear,
 158 and not by change in the static stability (not shown). On the other side of the basin, northwest of the
 159 Iberian peninsula, an increase in baroclinicity accompanies the increase in stormtrack activity. This is
 160 consistent with the enhanced meridional temperature gradient and the accelerated zonal wind that
 161 increases the vertical wind shear: the wind (Fig. 2D) decreases on the west north Atlantic coast,
 162 consistently with the reduced stormtrack, while it is shifted southwards on the east of the basin. Note that
 163 the southward shift of the jet stream at that location was already documented for the more recent period
 164 starting in 1979 by Simmons (2022). The same analysis as in Fig. 2 has been repeated with no substantial
 165 differences for the period 1979-2022 and for the upper layer 250-500 hPa. See Fig. S4 and S5.
 166



168 *Figure 2. A) Visualization of the summer storm-track as standard deviation of high-frequency of*
 169 *geopotential height at 500 hPa. Mean field for JJA in the period 1950-2022 in contour. In color the linear*
 170 *trend on JJA yearly mean fields expressed as meters per decade periods. B) Eady growth rate in the 500-*
 171 *850 hPa layer. As in A, the black contours are the mean field expressed in days^{-1} , in color is the linear*
 172 *trend in this case expressed as days^{-1} per decade period. C) Skin temperature: linear trend in Kelvin*
 173 *per 10 y period. D) Linear trend of the 500 hPa zonal wind in meters per second per decade. The mean*
 174 *field for the whole period is in contours. In all panels the areas of trend significant to a Mann-Kendall*
 175 *test with $p < 0.05$ are stippled.*
 176

177 **4 Eastern Atlantic depression increase**

178 In this section, a region straddling the area of positive trend seen in Fig. 1 is selected, shown as a green
 179 rectangle, and the deep depressions (DDs) occurring inside this region are counted. The relation of these
 180 events to Western European temperature is also computed. The region spans longitudes 14°W to 29°W
 181 and latitudes 38°N to 59°N . As before, this region is scanned by partially overlapping squares of 15
 182 degrees in longitude-latitude. The difference here is that when a deep depression is found in a given day
 183 for at least one of the squares, the day is retained as a deep depression day (DD-day) for the whole region;
 184 this allows harnessing more events.

185 A total of 724 DD-days were found for the whole period in the region, which corresponds to around 10
 186 days per summer on average – summer counting 92 days – although large year to year variations are
 187 present, as will be shown below. There is no seasonal cycle, the number of DD-days is not significantly
 188 different in either of the three summer months (not shown).

189 A composite map of the DD-days anomalies is shown for illustration in the supplementary material,
 190 Fig.S7. The synoptic structures of the selected depressions can be either cut off from the core of the
 191 westerly flow, or can be large troughs embedded in the jet. In Fig.S8 and Fig.S9 there are examples of the
 192 two: the cut off lows in June 2019 that were associated with a strong heatwave, and the deep troughs of
 193 August 2012. A simple criterion can be added to the DD definition in order to distinguish between the
 194 two kinds, checking the latitudinal position of the minimum z_{500} with respect to the position of the jet.
 195 This analysis (not shown) gives 17% of DD-days due to cut-off lows; both kinds show a significant
 196 increasing trend and only fine differences with respect to what shown in Fig. 3, so for the moment both
 197 will be considered indifferently. For a climatology and dynamics of cut-off lows see Nieto et al (2005).
 198 The bar plot in Fig. 3A shows the count of DD-days between 1950 and 2022 in ERA5. A positive trend
 199 and a large year-to-year variability are visible. The linear trend is highly significant to a Mann-Kendall
 200 test with a p-value $p = 2 \cdot 10^{-4}$ and almost doubles the number of DD-days across the 73 years period,
 201 consistently with Fig. 1. The average number of DD-days per summer is 7.6 in the period 1950-1974 and
 202 12 in the period 1998-2022. The linear trend computed from the NCEP reanalysis is also shown by the
 203 dashed line. The two reanalyses have the same linear trend, while NCEP counts approximately one DD-
 204 day less per summer; a more detailed comparison can be found in sec. 2 of the supplementary material.
 205 We construct the composite maps of 2-meters temperature at 14:00 UTC (2mT) by averaging 2mT
 206 anomaly fields for all 724 DD-days; to reduce the impact of global warming, the 2mT time series has
 207 been linearly detrended before computing the composite. This avoids putting more weights on the end of
 208 the period, when temperatures are higher and DD-days more frequent. The resulting pattern is in Fig. 3B,
 209 where practically all areas of continental Europe are statistically significant to a t-test with $p < 0.05$. It can
 210 be seen that DDs in the region are accompanied by high temperatures in central-western Europe. The
 211 pattern in Fig. 3B resembles closely the pattern of excess extreme heating of Vautard et al (2023, Fig.
 212 1.A), as well as the typical anomalous temperature pattern during West-European heatwaves (Stefanon et
 213 al 2012, Fig. 2).

214 This composite pattern hints at a relevance of the DD to extreme temperatures in western Europe, but a
 215 quantitative analysis of this relevance is deferred to a future paper. Here, we limit ourselves to estimating
 216 the effect of the increase of DD-days on the mean 2mT. This can be done by comparing the trend of 2mT

217 during the non-DD-days to the total trend: the difference is the contribution of the increase of DD-days.
218 For the area delimited by the green rectangle in Fig. 3B, the difference between these trends is 0.03
219 K/10y, which brings about a total excess mean heating of 0.2 K along the ERA5 73 years period. Given
220 that the total increase of 2mT at 14:00 in the same period is 3.4 K, we can say that the contribution,
221 though statistically significant, is small. See Figures S10 and S11 in the supplementary material.
222

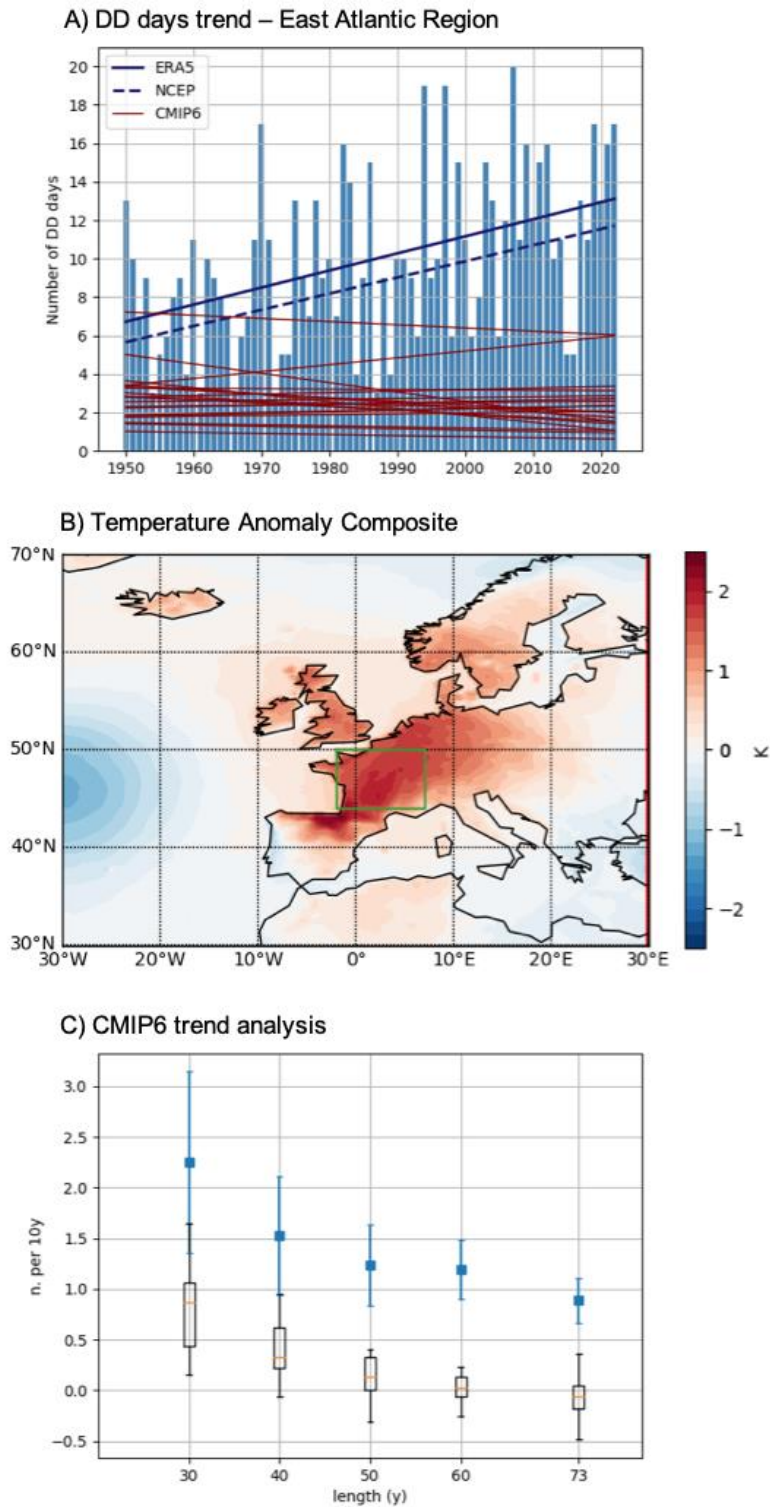
223 **5 Deep Depressions in CMIP6 models**

224

225 A sample of 20 historical integrations from 20 different models has been selected, and geopotential height
226 daily output at 500 hPa has been analyzed. The same procedure as in section 4 has been applied to the
227 model outputs, their results are represented superposed to those of ERA5 in Fig. 3A; the yearly bars are
228 not plotted for the models, only the estimated linear trend is displayed as the thin dark red lines. In
229 general models have a lower mean count of DD-days compared to ERA5, and only one simulation yields
230 a positive trend, but it is not significant.

231 In Fig. 3C the trends in the number of depressions is explored for shorter durations of time. The
232 maximum positive trend found for the durations of 30 to 73 years - included in the 1950-2022 period - are
233 shown in the figure, as a function of the trend length. The results for ERA5 are compared to the
234 distribution of the CMIP6 models trends. CMIP6 models do not manage to reproduce the positive trends
235 detected in the reanalyses, and their difference with ERA5 seems to increase with the length considered.
236 It is not surprising that the number of DD-days is underestimated in CMIP6 models. Harvey et al. (2020)
237 documented a weakening and northward shift of the summertime stormtrack in the subsequent
238 generations of CMIP models including the 6th. A weakening of blocking frequency is equally found by
239 Davini and D'Andrea (2020). Different reasons have been brought forward to explain this decreasing
240 variability; they include low spatial resolution (Zappa et al., 2013), orography (Berckmans et al., 2013),
241 or biases in surface temperature (Keeley et al., 2012).

242 While it would be useful to analyze each individual model in order to identify the dynamical origin of its
243 own reduced variability, a quick test can be carried out reducing the parameter A, i.e. the depth of the
244 z500 minima, in order to account for the reduced variability and increase the mean number of DD-days
245 found. The equivalent of figures 3A and 3C are found in the supplementary material Figures S12 and S13,
246 for A=70m. With this choice, the mean number of DD-days in the models is approximately equivalent to
247 ERA5, but still no model matches the increasing trend, with the exception of MPI-ESM1-2-HR that has a
248 significant positive trend with $p=0.04$. The individual behavior of each model is also displayed in Figure
249 S41. In Fig. S15 the same as Fig. 1 is represented for each model individually, still in this "boosted"
250 configuration using A=70m. Some models have marginally significant trends, most of the time negative
251 in different regions. IPSL-CM6A-LR reproduces the decrease of DD-days in the western Atlantic region
252 but not the increase in the East. The only – but little significant - models that have a pattern of DD trends
253 resembling ERA5 are ACCESS-CM2 and MPI-ESM1-2-HR.



254
255

256 *Figure 3. A) Bars: number of DD-days per summer in ERA5 in the Eastern Atlantic region shown in*
 257 *green in Fig. 1; linear interpolation in dark blue. Dark red lines are the result of the same analysis on a*
 258 *sample of CMIP6 models outputs, only the linear interpolation is shown, dark blue dashed is the same for*

259 *the NCEP reanalysis; see text Sec.5. B) Composite map of detrended 2 meters temperature anomaly at*
260 *14:00 UTC for all DD-days. The green box is the region for which the DD-days contribution to the mean*
261 *temperature is computed (see text). C) Maximum value of the linear trend for different period lengths.*
262 *Blue: ERA5 with 95% confidence interval. Box-whiskers plot : CMIP6 models. Trends are expressed as*
263 *the number of DD-days per decade.*
264

265 **6 Summary and discussion**

266 A simple algorithm for counting events of deep depression has been applied to the North
267 Atlantic/European region. The number of Deep Depressions (DD) days during summer has almost
268 doubled in the eastern Atlantic region since 1950. Such a trend has not been shown in preceding studies:
269 there is some consensus of an increase of storminess at high latitudes in the eastern north Atlantic, and of
270 a decrease south of it, off the British Isles, although not specifically in summer (see Freser et al 2015 and
271 references therein). But a direct comparison with the present work is not straightforward, for here we seek
272 depressions at a higher level in the troposphere. The same algorithm applied to ERA5 data has also been
273 applied to a sample of CMIP6 model outputs, and no trend is found, in agreement with recent storminess
274 analysis like Priestley and Catto (2022).
275 DD-days are accompanied by higher temperatures in western and central Europe, with a pattern that has
276 been linked to temperature extremes in previous literature. While the effect of the increase of Atlantic
277 depressions is limited on the mean summer 2mT in the western European region, this study suggests that
278 it could be relevant for the increase of heatwaves, via southerly temperature advection or other
279 mechanisms. The failure of CMIP6 models to reproduce this increase can consequently be linked to the
280 incorrect reproduction of these dynamical features or to a large-scale perturbation at the origin of both
281 phenomena. This is in good agreement with studies like Vautard et al. (2023) and Faranda et al. (2023).
282 Despite some consistent dynamical context of the increase of DDs given in this paper, an explanation of
283 the reasons for the phenomenon remains insufficient. It is moreover unclear whether the trend comes from
284 natural variability of the midlatitude flow or whether it is due to some large-scale forcing, of natural or
285 human-induced origin. Going back to Fig. 1 of this paper, while it is reasonable to think that the surface
286 warming on the American continent decreases the jetstream and the stormtrack in the western Atlantic, it
287 is less clear why there is an increase of activity in the eastern side. The increase in baroclinicity there is
288 due to an increase of the vertical shear of the wind and not to a change in vertical stability (not shown).
289 The increased vertical shear is associated with a southeastward shift of the jet. The causal relation of the
290 increased wind speed with the presence of increased cyclones in the area remains however undecided.
291 Other aspects of the summer midlatitude circulation are undergoing rapid modifications in reanalyzed
292 data. A strong positive trend has been observed for instance in the number of Greenland blocking events.
293 This increase has been suggested as a cause for Greenland continental temperature increase and ice
294 depletion (Hörhold et al., 2023 and references therein), but a dynamical understanding of this
295 phenomenon is still absent. Furthermore, Dong et al (2013) also found a southward shift of the Atlantic
296 stormtrack activity and changes of baroclinicity similar to Fig. 2B, and linked those to the Greenland
297 blocking increase. In addition, it is notable that CMIP6 models also fail in reproducing the Greenland
298 blocking increase (Davini and D'Andrea, 2020).
299 There have been advances in explaining the dynamics of the increase of heatwaves (see e.g. Hoffman et
300 al., 2021) and other kinds of persistent anomalies causing hydroclimatic extrema, but it is fair to say that a
301 full picture is still not available. Arctic Amplification has been proposed as a possible large-scale forcing
302 for weakening of summer storm tracks (Coumou et al., 2015), but aerosol forcings could also play a role
303 (Dong et al., 2022). Different mechanisms have been proposed in driving quasi-stationary Rossby waves,
304 including waveguide-effects, (Kornhuber et al., 2017), soil-moisture depletion (Teng & Branstator, 2019)
305 and zonally asymmetric thermal forcing (Moon et al., 2022). Whether or not such quasi-stationary waves
306 are increasing is debated but there are indications for an increase in wave number 5 (Teng et al., 2022)
307 and associated zonal-mean double-jet states (Rousi et al., 2022).

308 A number of ideas originating from this work deserve further research. First of all, the relevance of the
309 DD increase on extreme temperature has to be quantified. In fact, recent summer heatwaves (such as in
310 2022 or 2019) have been accompanied by persistent cut-off low patterns. This analysis is deferred to a
311 forthcoming paper. DDs or cut-off lows are not the only patterns creating heatwaves, of course: persistent
312 high-pressure systems over the western European regions are also very common. It will be interesting to
313 study in detail the interaction between DDs and high-pressure systems over continental Europe. As
314 discussed in the introduction, DDs can create high-pressure systems at mid troposphere by the increase of
315 temperature in the atmospheric column, and that could actually cause or reinforce a blocking. A high
316 pressure over continental Europe would have a local warming effect but also slow down the low-pressure
317 systems themselves, in the eastern Atlantic region. The analysis presented here does not allow the
318 detection of a significant increase with time of the duration of the DD events; however, it cannot be
319 excluded that the increase of temperature in western Europe could be the cause of the increase of DD over
320 the eastern Atlantic, rather than the effect. As highlighted by Drouard and Woolings (2018) DD can be
321 anticipated by the blocking anticyclone. No long-term trend in atmospheric blocking occurrence is found
322 over western Europe, but an increasing trend in z500 is indeed documented, see e.g. Simmons (2022).
323 Dedicated climate model experiments might be used to disentangle this causal relation. In any case, it is
324 notable that the very fact that CMIP6 models do not reproduce the trend of DD-days nor the excess
325 heating of western Europe is an additional hint of the link between the two phenomena. A more refined
326 analysis on the CMIP6 models that do (like MPI-ESM1-2-HR) or do not reproduce the trend could also
327 give information on the causal relation between high-pressure over Europe and DDs.
328 Whether it is internal or forced variability, it remains clear that CMIP6 models appear to be unable to
329 correctly reproduce the complex dynamical changes happening in the northern extratropical summer,
330 which is likely part of the explanation of the insufficient prediction of increase in western European
331 extreme temperatures. Great caution should be consequently used when analyzing climate change
332 predictions in the region, and even more so when studying changes in complex dynamical phenomena.

333 **Acknowledgments**

334 Two anonymous reviewers largely contributed to improving the manuscript. FDA thanks Paolo Davini
335 for advice and discussion. RV, DC, DF, TH and PY acknowledge funding from the European Union's
336 H2020 program grant agreement 101003469 (XAIDA).

337 **Open Research (Data Availability Statement).**

338 All data used is open and publicly available :

339 ERA5 data is available at Hersbach et al (2023).

340 NCEP-NCAR Reanalysis data is available at Kalnay et al (1996)

341 CMIP6 data are available from any node of the Earth System Grid Federation (ESGF), see Cinquini et al
342 (2014).

343 We acknowledge the use of the open source scientific environment spyder : Raybaut, P. (2009).

344 **References**

- 345 Bador, M., Terray, L., and Boé, J. (2016), Emergence of human influence on summer record-breaking
346 temperatures over Europe, *Geophys. Res. Lett.*, 43, 404–412, doi:10.1002/2015GL066560.
347
- 348 Berckmans, J., Woollings, T., Demory, M.-E., Vidale, P.-L., & Roberts, M. (2013). Atmospheric
349 blocking in a high resolution climate model: Influences of mean state, orography and eddy forcing.
350 *Atmospheric Science Letters*, 14, 34–40. <https://doi.org/10.1002/asl2.412>
351
- 352 Boé, J., Terray, L., Moine, M. P., Valcke, S., Bellucci, A., Drijfhout, S., ... & Wyser, K. (2020). Past long-
353 term summer warming over western Europe in new generation climate models: role of large-scale
354 atmospheric circulation. *Environmental Research Letters*, 15(8), 084038.
355
- 356 Cinquini, L., Daniel Crichton, Chris Mattmann, John Harney, Galen Shipman, Feiyi Wang, Rachana
357 Ananthakrishnan, Neill Miller, Sebastian Denvil, Mark Morgan, Zed Pobre, Gavin M. Bell, Charles
358 Doutriaux, Robert Drach, Dean Williams, Philip Kershaw, Stephen Pascoe, Estanislao Gonzalez, Sandro
359 Fiore, Roland Schweitzer, The Earth System Grid Federation: An open infrastructure for access to
360 distributed geospatial data, *Future Generation Computer Systems*, Volume 36, 2014, Pages 400-417,
361 ISSN 0167-739X, <https://doi.org/10.1016/j.future.2013.07.002>. [dataset] [https://esgf-](https://esgf-node.ipsl.upmc.fr/search/cmip6-ipsl/)
362 [node.ipsl.upmc.fr/search/cmip6-ipsl/](https://esgf-node.ipsl.upmc.fr/search/cmip6-ipsl/).
363
- 364 D. Coumou, J. Lehmann, J. Beckmann, The weakening summer circulation in the Northern Hemisphere
365 mid-latitudes. *Science* **348**, 324–327 (2015).
366
- 367 Davini, P., F D'Andrea 2020 : From CMIP3 to CMIP6: Northern Hemisphere atmospheric blocking
368 simulation in present and future climate *Journal of Climate* 33 (23), 10021-10038
- 369 Deng, Kai-Qiang, Cesar Azorin-Molina, Song Yang, Chun-Di Hu, Gang-Feng Zhang, Lorenzo Minola,
370 Sergio Vicente-Serrano, Deliang Chen, 2022: Shifting of summertime weather extremes in Western Europe
371 during 2012–2020, *Advances in Climate Change Research*, Volume 13, Issue 2. 218-227, ISSN 1674-9278,
372 <https://doi.org/10.1016/j.accre.2022.01.008>.
- 373 Dong, B., R.T. Sutton, T. Woollings, K. Hodges 2013: Variability of the North Atlantic summer storm
374 track: mechanisms and impacts on European climate *Environ. Res. Lett.* 8 (2013) 034037 (9pp)
375 10.1088/1748-9326/8/3/034037
- 376 Dong S, Sun Y and Li C 2020 Detection of human influence on precipitation extremes in Asia *J. Clim.* **33**
377 5293–304
- 378 Drouard, M., and T. Woollings, 2018: Contrasting Mechanisms of Summer Blocking Over Western
379 Eurasia. *Geophysical Research Letters*, 45(21), 12,040-012,048, <https://doi.org/10.1029/2018GL079894>.
380
- 381 Eyring, V., S. Bony, G. A. Meehl, C. A. Senior, B. Stevens, R. J. Stouffer, and K. E. Taylor, 2016: Overview
382 of the Coupled Model Intercomparison Project phase 6 (CMIP6) experimental design and organization.
383 *Geosci. Model Dev.*, 9, 1937–1958, <https://doi.org/10.5194/gmd-9-1937-2016>.
384
- 385 Faranda, D., G. Messori, A. Jezequel, M. Vrac, P. Yiou: Atmospheric circulation compounds
386 anthropogenic warming and impacts of climate extremes in Europe. *Proceedings of the National Academy*
387 *of Sciences* March 21, 2023, 120 (13) e2214525120 <https://doi.org/10.1073/pnas.2214525120>
388

- 389 Feser, F., Barcikowska, M., Krueger, O., Schenk, F., Weisse, R. and Xia, L. (2015), Storminess over the
 390 North Atlantic and northwestern Europe—A review. *Q.J.R. Meteorol. Soc.*, 141: 350-382. [https://doi-
 392 org.insu.bib.cnrs.fr/10.1002/qj.2364](https://doi-

 391 org.insu.bib.cnrs.fr/10.1002/qj.2364)
- 393 Harvey, B. J., Cook, P., Shaffrey, L. C., & Schiemann, R. (2020). The response of the northern hemisphere
 394 storm tracks and jet streams to climate change in the CMIP3, CMIP5, and CMIP6 climate models. *Journal
 395 of Geophysical Research: Atmospheres*, 125, e2020JD032701. <https://doi.org/10.1029/2020JD032701>
 396
- 397 Hersbach, H., Bell, B., Berrisford, P., Biavati, G., Horányi, A., Muñoz Sabater, J., Nicolas, J., Peubey, C.,
 398 Radu, R., Rozum, I., Schepers, D., Simmons, A., Soci, C., Dee, D., Thépaut, J.-N. (2023): ERA5 hourly
 399 data on pressure levels from 1940 to present. Copernicus Climate Change Service (C3S) Climate Data Store
 400 (CDS), DOI: [10.24381/cds.bd0915c6](https://doi.org/10.24381/cds.bd0915c6) [dataset]
- 401 Kalnay et al., The NCEP/NCAR 40-year reanalysis project, *Bull. Amer. Meteor. Soc.*, 77, 437-470, 1996
 402 [dataset] <https://psl.noaa.gov/data/gridded/data.ncep.reanalysis.html>
- 403 Hoffmann, P., Jascha Lehmann, Bijan H. Fallah, Fred F. Hattermann (2021): Atmosphere similarity
 404 patterns in boreal summer show an increase of persistent weather conditions connected to hydro-climatic
 405 risks. *Nature Scientific Reports*. [DOI: 10.1038/s41598-021-01808-z]
- 406 Hörhold, M., Münch, T., Weißbach, S. *et al.* Modern temperatures in central–north Greenland warmest in
 407 past millennium. *Nature* **613**, 503–507 (2023). <https://doi.org/10.1038/s41586-022-05517-z>
 408
- 409 Hoskins Brian J and Paul J Valdes. On the existence of storm-tracks. *Journal of the atmospheric sciences*,
 410 47(15):1854–1864, 1990.
- 411
- 412 Keeley, S., Sutton, R., & Shaffrey, L. (2012). The impact of North Atlantic Sea surface temperature errors
 413 on the simulation of North Atlantic European region climate. *Quarterly Journal of the Royal
 414 Meteorological Society*, 138, 1774– 1783. <https://doi.org/10.1002/qj.1912>
- 415 Kornhuber, K., Petoukhov, V., Karoly, D., Petri, S., Rahmstorf, S., & Coumou, D. (2017). Summertime
 416 Planetary Wave Resonance in the Northern and Southern Hemispheres, *Journal of Climate*, 30(16), 6133-
 417 6150.
- 418 Lindzen, R. S. & Farrell, B. A 1980: simple approximate result for the maximum growth rate of baroclinic
 419 instabilities. *J. Atmos. Sci.* **37**, 1648–1654
- 420 Moon, W., Kim, B.-M., Yang, G.-H. & Wettlaufer, 2022: Wavier jet streams driven by zonally asymmetric
 421 surface thermal forcing *J. S. Proc. Natl Acad. Sci. USA* **119**, e2200890119 .
- 422 Nieto, R., and Coauthors, 2005: Climatological Features of Cutoff Low Systems in the Northern
 423 Hemisphere. *J. Climate*, **18**, 3085–3103, <https://doi.org/10.1175/JCLI3386.1>.
- 424 Priestley, M. D. K. and Catto, J. L.: Future changes in the extratropical storm tracks and cyclone intensity,
 425 wind speed, and structure, *Weather Clim. Dynam.*, 3, 337–360, <https://doi.org/10.5194/wcd-3-337-2022>,
 426 2022.
- 427 Raible, C. C., P. M. Della-Marta, C. Schwierz, H. Wernli, and R. Blender, 2008: Northern Hemisphere
 428 Extratropical Cyclones: A Comparison of Detection and Tracking Methods and Different Reanalyses. *Mon.
 429 Wea. Rev.*, **136**, 880–897, <https://doi.org/10.1175/2007MWR2143.1>.
 430

- 431 Raybaut, P. (2009). Spyder-documentation. Available Online at: *Pythonhosted.Org*. [software]
432 <https://www.spyder-ide.org/>
433
- 434 Ribes, A., Boé, J., Qasmi, S., Dubuisson, B., Douville, H., & Terray, L. (2022). An updated assessment of
435 past and future warming over France based on a regional observational constraint. *Earth System Dynamics*
436 *Discussions*, 1-29.
437
- 438 Rousi, E., Kornhuber, K., Beobide-Arsuaga, G. *et al.* Accelerated western European heatwave trends linked
439 to more-persistent double jets over Eurasia. *Nat Commun* **13**, 3851 (2022). [https://doi.org/10.1038/s41467-](https://doi.org/10.1038/s41467-022-31432-y)
440 [022-31432-y](https://doi.org/10.1038/s41467-022-31432-y)
441
- 442 Simmons, A. J.: Trends in the tropospheric general circulation from 1979 to 2022, *Weather Clim. Dynam.*,
443 *3*, 777–809, <https://doi.org/10.5194/wcd-3-777-2022>, 2022.
444
- 445 Schumacher, D. L., Hauser, M., & Seneviratne, S. I. (2022). Drivers and mechanisms of the 2021 Pacific
446 Northwest heatwave. *Earth's Future*, *10*, e2022EF002967. <https://doi.org/10.1029/2022EF002967>
447
- 448 M Stefanon, F D'Andrea, P Drobinski 2012: Heatwave classification over Europe and the Mediterranean
449 region. *Environmental Research Letters* *7* (1), 014023
450
- 451 Teng, H., Branstator, G. Amplification of Waveguide Teleconnections in the Boreal Summer. *Curr Clim*
452 *Change Rep* **5**, 421–432 (2019). <https://doi.org/10.1007/s40641-019-00150-x>
453
- 454 Teng, H., R. Leung, G. Branstator, J. Lu, and Q. Ding, 2022: Warming Pattern over the Northern
455 Hemisphere Midlatitudes in Boreal Summer 1979–2020. *J. Climate*, **35**, 3479–3494,
456 <https://doi.org/10.1175/JCLI-D-21-0437.1>.
457
- 458 van Oldenborgh, G. J., Drijfhout, S., van Ulden, A., Haarsma, R., Sterl, A., Severijns, C., Hazeleger, W.,
459 and Dijkstra, H.: Western Europe is warming much faster than expected, *Clim. Past*, *5*, 1–12,
460 <https://doi.org/10.5194/cp-5-1-2009>, 2009.
461
- 462 Van Oldenborgh, G. J., Wehner, M. F., Vautard, R., Otto, F. E. L., Seneviratne, S. I., Stott, P. A., et al.
463 (2022). Attributing and projecting heatwaves is hard: We can do better. *Earth's Future*, *10*,
464 e2021EF002271. <https://doi.org/10.1029/2021EF002271>
465
- 466 Vautard, R., J. Cattiaux, T. Happé, J. Singh, R. Bonnet, C. Cassou, D. Coumou, F. D'Andrea, Davide
467 Faranda, E. Fischer, A. Ribes, S. Sippel, P. Yiou, 2023 : Heat extremes in Western Europe are increasing
468 faster than simulated due to missed atmospheric circulation trends. *Nature Comm.*, **14**, 6803 (2023).
469 <https://doi.org/10.1038/s41467-023-42143-3>
470
- 471 Wilks, D. S., 2016: “The Stippling Shows Statistically Significant Grid Points”: How Research Results
472 are Routinely Overstated and Overinterpreted, and What to Do about It. *Bull. Amer. Meteor. Soc.*, **97**,
473 2263–2273, <https://doi.org/10.1175/BAMS-D-15-00267.1>.
474
- 475 Zappa, G., Shaffrey, L. C., & Hodges, K. I. (2013). The ability of CMIP5 models to simulate North
476 Atlantic extratropical cyclones. *Journal of Climate*, *26*, 5379– 5396. [https://doi.org/10.1175/JCLI-D-12-](https://doi.org/10.1175/JCLI-D-12-00501.1)
477 [00501.1](https://doi.org/10.1175/JCLI-D-12-00501.1)
478
- 479 Zschenderlein, P, Fink, AH, Pfahl, S, Wernli, H. Processes determining heat waves across different
480 European climates. *Q J R Meteorol Soc* 2019; 145: 2973- 2989. <https://doi.org/10.1002/qj.3599>